Cite as: S. I. Kim *et al.*, *Sci. Transl. Med.* 10.1126/scitranslmed.abd6990 (2021).

CORONAVIRUS

Stereotypic neutralizing V_H antibodies against SARS-CoV-2 spike protein receptor binding domain in COVID-19 patients and healthy individuals

Sang Il Kim[1,2†], Jinsung Noh[3†], Sujeong Kim[1,4], Younggeun Choi[1], Duck Kyun Yoo[1,2,4], Yonghee Lee[3], Hyunho Lee[3], Jongtak Jung[5], Chang Kyung Kang[5], Kyoung-Ho Song[5], Pyoeng Gyun Choe[5], Hong Bin Kim[5], Eu Suk Kim[5], Nam-Joong Kim[5], Moon-Woo Seong[6], Wan Beom Park[5], Myoung-don Oh[5], Sunghoon Kwon[3,7,8,9,10*], and Junho Chung[1,4,11*]

[1]Department of Biochemistry and Molecular Biology, Seoul National University College of Medicine, Seoul 03080, Republic of Korea. [2]Ischemic/Hypoxic Disease Institute, Seoul National University Medical Research Center, Seoul 03080, Republic of Korea. [3]Department of Electrical and Computer Engineering, Seoul National University, Seoul 08826, Republic of Korea. [4]Department of Biomedical Science, Seoul National University College of Medicine, Seoul 03080, Republic of Korea. [5]Department of Internal Medicine, Seoul National University College of Medicine, Seoul 03080, Republic of Korea. [6]Department of Laboratory Medicine, Seoul National University College of Medicine, Seoul 03080, Republic of Korea. [7]Interdisciplinary Program in Bioengineering, Seoul National University, Seoul 08826, Republic of Korea. [8]BK21+ Creative Research Engineer Development for IT, Seoul National University, Seoul 08826, Republic of Korea. [9]Biomedical Research Institute, Seoul National University Hospital, Seoul 03080, Republic of Korea. [10]Institutes of Entrepreneurial BioConvergence, Seoul National University, Seoul 08826, Republic of Korea. [11]Cancer Research Institute, Seoul National University College of Medicine, Seoul 03080, Republic of Korea.

†These authors contributed equally to this work.

*To whom correspondence should be addressed. **Email:** skwon@snu.ac.kr (S.K.); jjhchung@snu.ac.kr (J.C.)

Stereotypic antibody clonotypes exist in healthy individuals and may provide protective immunity against viral infections by neutralization. We observed that 13 out of 17 patients with COVID-19 had stereotypic variable heavy chain (V_H) antibody clonotypes directed against the receptor-binding domain (RBD) of SARS-CoV-2 spike protein. These antibody clonotypes were comprised of immunoglobulin heavy variable (IGHV)3-53 or IGHV3-66 and immunoglobulin heavy joining (IGHJ)6 genes. These clonotypes included IgM, IgG_3, IgG_1, IgA_1, IgG_2, and IgA_2 subtypes and had minimal somatic mutations, which suggested swift class switching after SARS-CoV-2 infection. The different immunoglobulin heavy variable chains were paired with diverse light chains resulting in binding to the RBD of SARS-CoV-2 spike protein. Human antibodies specific for the RBD can neutralize SARS-CoV-2 by inhibiting entry into host cells. We observed that one of these stereotypic neutralizing antibodies could inhibit viral replication in vitro using a clinical isolate of SARS-CoV-2. We also found that these V_H clonotypes existed in six out of 10 healthy individuals, with IgM isotypes predominating. These findings suggest that stereotypic clonotypes can develop de novo from naïve B cells and not from memory B cells established from prior exposure to similar viruses. The expeditious and stereotypic expansion of these clonotypes may have occurred in patients infected with SARS-CoV-2 because they were already present.

INTRODUCTION

Stereotypic antibodies (Abs), which share similar sequences across multiple individuals, can be produced in response to immunological stimulation upon infection. A subset of stereotypic neutralizing Abs (nAbs) encoded by naïve B cells that have not undergone somatic hypermutation and class switching from IgM or IgD isotypes are of great interest (*1*, *2*) because their origin effectively excludes the possibility that these nAbs evolved from pre-existing clonotypes that are reactive to similar viruses. This phenomenon is referred to as original antigenic sin (OAS) and has been linked to antibody-dependent enhancement (ADE) of viral infections, which can be potentially fatal, as observed during the development of experimental dengue virus vaccines (*3*–*6*). Several groups have identified nAbs for severe acute respiratory syndrome coronavirus 2 (SARS-CoV-2) (*7*–*11*), and one report suggests that stereotypic nAbs using germline immunoglobulin heavy variable (IGHV)*3-53* and IGHV*3-66* genes may exist among convalescent COVID-19 patients (*7*). The structural basis of the stereotypic nAb reaction to SARS-CoV-2 has been clarified with the cocrystal structure of two IGHV*3-53* nAbs in complex with the SARS-CoV-2 receptor-binding domain (RBD), which defines the critical germline-encoded residues in the binding site of angiotensin-

converting enzyme II (ACE2), the functional receptor of SARS-CoV-2 (*12*). The prevalence of these stereotypic nAb clonotypes among SARS-CoV-2 patients and their characteristics, such as frequency within immunoglobulin (Ig) repertoires, somatic mutations, isotypes, and chronological changes remain to be elucidated.

Here, we report stereotypic nAb clonotypes for SARS-CoV-2, which were identified by mapping nAbs onto deep Ig repertoires that were profiled from infected patients. The stereotypic-naïve nAb clonotypes encoded by the IGHV3-53/IGHV3-66 and immunoglobulin heavy joining (IGHJ)6 genes existed in the majority of convalescent COVID-19 patients and showed little evidence of somatic mutations along with swift isotype class switching to IgG_1, IgA_1, and even IgA_2 subtypes. Subsequently, we found that these same variable heavy chain (V_H) clonotypes pre-exist predominantly as an IgM isotype in healthy individuals, possibly encoded by naïve B cells, which suggests that these stereotypic nAbs are not originated from clonotypes developed by previous infection with similar viruses. Individuals with these V_H clonotypes are may be able to rapidly produce potent nAbs and potentially afford partial protection against SARS-CoV-2.

RESULTS

Isolation and characterization of human nAbs

To obtain monoclonal nAbs against SARS-CoV-2, we collected blood samples from 17 SARS-CoV-2-infected patients (Patients A–Q), which were used to generate human antibody libraries. SARS-CoV-2 also uses spike (S) protein for receptor binding and membrane fusion in a mechanism similar to SARS-CoV (*13*) and requires binding with cellular receptor ACE2 to gain entry into the host cell (*14*, *15*). A previous report suggests that a human monoclonal antibody (mAb) that reacts with the RBD within the S1 region of the S protein can hinder the initial binding interaction between the virus and the cell, effectively neutralizing SARS-CoV-2 (*11*). We confirmed the reactivity of convalescent patient sera with recombinant SARS-CoV-2 S and RBD proteins. Patients A and E, who presented with extensive pneumonic infiltrates, also showed high plasma IgG titers against recombinant SARS-CoV-2 nucleocapsid (N), S, S1, S2, and RBD proteins, which was detected 11, 17, and 45 days after symptom onset in Patient A and 23, 44, and 99 days after symptom onset in Patient E (Table S1 and Fig. 1). Sera samples from Middle East respiratory syndrome coronavirus (MERS-CoV) patients crossreacted with the SARS-CoV-2 S protein, showed a higher titer against the S2 domain and crossreactivity to MERS-CoV S2 was detected in SARS-CoV-2 sera samples (Figs. 1 and S1), suggesting the potential risk for ADE. We generated four human Ab libraries using a phage-display system, based on the blood samples from Patient A, which were collected on days 17 and 45 (A_d17 and A_d45), and Patient E, which were collected on days 23 and 44 (E_d23 and E_d44). We isolated 38 single-chain variable fragment (scFv) clones that were reactive against recombinant SARS-CoV-2 RBD as measured with SARS-CoV-2 RBD-specific enzyme-linked immunosorbent assay (ELISA) (Figure S2 and Table S2). The half-maximal binding of scFv-human kappa light chain fragment (hC_K) to SARS-CoV-2 RBD occurred at concentrations ranging from 0.32 to 364 nM, which was comparable to findings in previous reports that have described human mAbs against the same protein (*8*, *11*). We tested whether these antibody clones could inhibit the binding between recombinant SARS-CoV-2 S protein and Vero E6 cells expressing the ACE2 receptor. A recombinant polyhistidine (HIS)-tagged SARS-CoV-2 S protein showed binding saturation at 200 nM when incubated with 1.5×10^5 Vero E6 cells, as measured using flow cytometry analysis with a fluorescein isothiocyanate (FITC)-labeled anti-HIS antibody. For the analysis of different scFv clones, recombinant S protein (200 nM) was mixed with scFv-hFc fusion proteins, at a final concentration of either 200 nM (equimolar) or 600 nM (molar ratio of 1:3). Eleven clones (A-1A1, A-1H4, A-1H12, A-2F1, A-2H4, A-2G3, E-3A12, E-3B1, E-3G9, E-3H31, and E-4D12) almost completely inhibited binding between recombinant S protein and Vero E6 cells at 600 nM, and some showed inhibitory activity at 200 nM (Figure S3). We used an in vitro viral neutralization assay in which Vero cells were infected with a clinical isolate of SARS-CoV-2 (BetaCoV/Korea/SNU01/2020) encoding D614 in the viral S protein at a medium tissue culture infectious dose ($TCID_{50}$) of 2,500 and in the presence of one of the 11 scFv-hC_K fusion proteins, at concentrations of 0.5, 5, or 50 μg/mL. Viral RNA concentrations in the culture supernatant were determined 0, 24, 48, and 72 hours after infection. Nine scFv-hC_K fusion proteins exhibited complete neutralizing activity at 50 μg/mL (Figure S4), and two antibodies (A-1H4 and E-3G9) showed potent neutralization even at 5 μg/mL (Figure S4). Five nAbs with IgG2/4 isotypes (E-3B1, A-1H4, A-2H4, A-2F1, and E-3G9) exhibited potent neutralizing activity against authentic SARS-CoV-2, with half-maximal inhibitory concentration (IC_{50}) ranging from 0.137 to 0.713 μg/mL (Fig. 2A).

Identification of stereotypic clonotypes from IGH repertoire of SARS-CoV-2-infected patients

We performed deep profiling of the Ig repertoire in three chronological blood samples each from Patients A and E, two chronological samples each from Patients B, C, D, F, and G, and a single time point sample from the remaining ten patients (H-Q). We searched for nAb clonotypes that possessed identical variable (V) and joining (J) gene combinations and perfectly matched heavy chain complementarity-determining region 3 (HCDR3) amino acid sequences among the immunoglobulin heavy chain (IGH) repertoires of Patients A and E. One and five nAb clonotypes that met these criteria were identified in Patients A and E, respectively (Fig. 2B), and three nAbs (A-2F1, E-3A12, and E-3B1) were encoded by

IGHV3-53/IGHV3-66 and IGHJ6 (Fig. 2B). These two V_H genes, IGHV3-53*01 and IGHV3-66*01 share an identical amino acid sequence, except for the H12 residue (isoleucine in IGHV3-53 and valine in IGHV3-66), and only five nucleotides differ between their sequences. Four clonotypes were IgG_1, and two clonotypes were class-switched to IgA_1 and IgA_2, when examined 44 days after symptom onset (Fig. 2B). These clonotypes had a very low frequency of somatic mutations (1.03% ± 0.51%), which was compatible with findings about other nAbs in previous reports (*7*, *8*). We evaluated all V_H sequences from the 17 patients and searched the clonotypes of 11 nAbs that were encoded by the same VJ genes and showed 66.6% or higher identity in the amino acid sequence for HCDR3 (Figure S5). Clonotypes that were highly homologous to the E-3B1 nAb were found among 13 out of 17 patients, with a total of 126 clonotypes having the isotype of IgG_3 (Patients I, K, and P), IgG_1 (Patients A, B, D-I, K, M, O, and P), IgA_1 (Patients E, G, I, and J), IgG_2 (Patients I-K) and IgA_2 (Patient E) (Table S3). These clonotypes shared nearly identical V_H sequences (92.45% ± 3.04% identity between amino acid sequences), with E-3B1 displaying an extremely low frequency of somatic mutations (0.98% ± 1.48%). Among these 126 clonotypes, 43 unique HCDR3s were identified by amino acid sequence, and 12 unique HCDR3s were present in more than one patient (Table 1).

Light chain plasticity of the stereotypic V_H clonotypes for binding to SARS-CoV-2 RBD

To test the reactivity of clonotypes homologous to E-3B1 against the SARS-CoV-2 S protein, we arbitrarily sampled 12 IGH clonotypes (Fig. 2C), containing five different HCDR3s, from the IGH repertoires of 13 patients. The genes encoding these IGH clonotypes were chemically synthesized and used to construct scFv genes with the variable lambda chain (V_λ) gene from the E-3B1 clone. The reactivity of these scFv clones to recombinant S and RBD was tested using a phage ELISA, and three clones (E-12, A-32, and B-33) reacted against recombinant S and RBD proteins (Fig. 2C). scFv libraries were constructed, using the A-11, A-31, E-34, A,B,G-42, G-44, D-51, F-53, E-52, and A-54 genes, and the variable kappa chain (V_κ)/V_λ genes amplified from Patients A, E, and G, and all 12 IGH clonotypes were reactive against both recombinant S and RBD proteins when paired with eight different V_κ and V_λ genes (Figs. 2C and 2D). All seven light chain-profiled patients (A–G) possessed these V_κ/V_λ clonotypes with identical VJ gene usage and perfectly matching light chain CDR3 (LCDR3) amino acid sequences (Figure S6). Immunoglobulin lambda variable (IGLV)2-14/immunoglobulin lambda joining (IGLJ)3, IGLV3-19/IGLJ2, and IGLV3-21/IGLJ2 were frequently used across all seven patients (Figures S7 and S8). Because E-3B1 effectively inhibited the replication of SARS-CoV-2 (Fig. 2A), these 126 clonotypes are likely to neutralize SARS-CoV-2 when paired with an optimal light chain.

Stereotypic-naïve IGH clonotype against SARS-CoV-2 pre-exist in the healthy population

Among IGH clonotypes, A,B,G-42 was unique, presenting little to no evidence of somatic mutations (0.6% ± 0.8%) and containing an HCDR3 (DLYYYGMDV) formed by the simple joining of IGHV3-53 and IGHJ6. This naïve V_H sequence existed in the IGH repertoire of five patients (Patients A, B, G, I, and K), as IgM and IgG_1, IgM and IgG_1, IgG_1 and IgA_1, IgM, or IgG_1 subtypes, respectively (Table 1). The IGH clonotypes encoded by IGHV3-53/IGHV3-66 and IGHJ6 that possessed an HCDR3 (DLYYYGMDV) with zero to one somatic mutation could be identified within the IGH repertoire of six of 10 healthy individuals, predominantly as an IgM isotype (*16*), based on publicly available IGH repertoires (Table 1). The A,B,G-42 clonotype showed light chain plasticity and could pair with five V_κ /V_λ genes to achieve RBD binding. In particular, the V_κ gene (2J6H) accumulated only five somatic mutations (1.4% divergence). None of the 12 clones, including A,B,G-42, reacted against the recombinant RBD proteins from either SARS-CoV or MERS-CoV (Figure S9). None of the 37 identified MERS-RBD-binding human mAbs (from two patients) were encoded by IGHV3-53/IGHV3-66 and IGHJ6 (Table S4) based on analysis of a prior study (*17*). Therefore, the presence of these stereotypic-naïve IGH clonotypes in the healthy population, and their light chain plasticity needed to achieve SARS-CoV-2 RBD binding, may be unique to SARS-CoV-2, which might provide a rapid and effective humoral response to the virus among patients who express these clonotypes. These findings suggest that a portion of the population possesses germline-precursor B cells, encoded by IGHV3-53/IGHV3-66 and IGHJ6, which can actively initiate virus neutralization upon SARS-CoV-2 infection.

Distinctive V and J gene usage of the SARS-CoV-2 RBD-binding antibodies

To further elucidate the preferential use of IGHV3-53/IGHV3-66 and IGHJ6 genes during the generation of SARS-CoV-2 RBD-binding antibodies, we extracted 252 predicted RBD-binding clones from our biopanning data. We previously showed that antibody clones with binding properties can be predicted by employing next-generation sequencing (NGS) technology and analyzing the enrichment patterns of biopanned clones (*18*, *19*). The IGHJ4 gene was more prominent within the IGH repertoires of 17 patients, similar to healthy human samples (*16*, *20*), but the predicted RBD-binding clones primarily used the IGHJ6 gene (Fig. 2E). Furthermore, the predicted RBD-binding clones showed the dominant usage of IGHV3-53/IGHJ6 and IGHV3-66/IGHJ6 pairs, which was not observed in the whole IGH repertoires of patients (Fig. 2F).

Chronological follow-up of IGH repertoire and the SARS-CoV-2 RBD-binding antibodies from patients

Naïve B cells typically undergo somatic hypermutations,

clonal selection, and class-switching following antigen exposure. We examined the chronological events that occurred in all IGH clonotypes identified in Patients A - G and those that were reactive against the SARS-CoV-2 RBD. In the entire patient IGH repertoire, naïve-derived IGH clonotypes with minimal somatic mutations (< 2.695% ± 0.700%) showed increased IgG_3 and IgG_1 subtypes, and the proportion of the IgG_1 subtype was dramatically increased for a period (Fig. 3A and 3B and Figure S10). The naïve-derived IGH clonotypes were detected as minor populations of IgA_1 and IgG_2 subtypes in Patients A and E (Figs. 3A and 3B), and as an IgA_2 subtype in Patient E (Fig. 3B). We categorized RBD-reactive clones into three groups: 1) neutralizing antibodies (neutralize), 2) binding-confirmed antibodies (bind), and 3) binding-predicted antibodies (predicted). In all three groups, these IGH clonotypes appeared and disappeared throughout the disease course, showed a low frequency of somatic mutations (Figs. 3C and 3D), and displayed rapid class-switching, especially to IgG_1, IgA_1, and IgA_2. These results suggest that RBD-reactive IGH clonotypes can emerge rapidly and undergo class-switching to IgG_1, IgA_1, and IgA_2, without accumulating many somatic mutations. This dramatic temporal surge of naïve IGH clonotypes, with rapid class-switching, occurred across the entire IGH repertoire of the patients and was not confined to those reactive to the SARS-CoV-2 RBD.

Selected nAbs retained its ability to bind to most current SARS-CoV-2 mutants

Several mutations within the S1 domain of the SARS-CoV-2 S protein have been identified during the 2019-20 global pandemic (*21*), thus we examined the probability of escape mutants emerging from the IGH repertoire induced by the wild-type virus infection. Our E-3B1, A-1H4, A-2F1, A-2H4, and E-3G9 nAbs successfully bound to different recombinant mutant S1 proteins (V341I, F342L, N354D, V367F, R408I, A435S, G476S, V483A, and D614G) in a dose-dependent manner, with compatible reactivity against recombinant wild-type S1 and RBD proteins (Fig. 4). Therefore, the human IGH immune repertoire may provide effective protection against an array of SARS-CoV-2 mutants.

DISCUSSION

In response to SARS-CoV-2 infection, some human IGH repertoires can efficiently generate clonotypes encoded by IGHV3-53/IGHV3-66 and IGHJ6, which can pair with diverse light chains, and form Abs with both RBD binding and virus neutralization properties. These clonotypes appear to have few to no somatic mutations and can undergo swift class-switching to IgG_1, IgA_1, and even IgA_2 subtypes. The expeditious development of these IGH clonotypes is possible because the naïve-stereotypic IGHV3-53/IGHV3-66 and IGHJ6 clonotypes pre-exist in a portion of the healthy population, predominantly as an IgM isotype. In line with our findings, several groups have reported potent human nAbs, composed of either IGHV3-53 or IGHV3-66 and IGHJ6 genes, using single B cell sequencing technology (*7*–*11*). The crystal structures of two IGHV3-53 nAbs has been determined, which has shown that two key motifs within HCDR1 and HCDR2 that are encoded in the IGHV3-53 germline can bind to SARS-CoV-2 S protein RBD (*12*). Therefore, the preferential use of IGHV3-53/IGHV3-66 and IGHJ6 in the development of nAbs to SARS-CoV-2 appears promising, especially given evidence that IGHV3-53/IGHV3-66 and IGHJ6 are able to pair with diverse light chains in order to form nAbs that can bind to the RBD. We found eight different light chains from our experiments, and other groups have identified nine different light chains (*12*). It is expected that the extent of light chain plasticity is broad enough for virus-exposed individuals to successfully evolve nAbs given that class-switched IGHV3-53/IGHV3-66 and IGHJ6 clonotypes were present in 13 of 17 patients from our study.

Currently, we do not know whether the stereotypic nAbs are polyreactive or autoreactive. Rather, our selected stereotypic nAbs, including A,B,G-42, do not appear to crossreact with recombinant RBD proteins of either SARS-CoV or MERS-CoV. Several reports have evaluated auto- or polyreactivity of SARS-CoV-2 nAbs with minimal somatic mutations, and one report showed that 18 nAbs, including four antibodies encoded by IGHV3-53/IGHJ4, IGHV3-53/IGHJ6, or IGHV3-66/IGHJ4, did not show evidence of being polyreactive or autoreactive (*22*). Another group characterized 29 Abs, including three nAbs encoded by IGHV3-53, with limited somatic mutations (<1.4%) and a HCDR3 length of 10 or 16 amino acids, and none of these Abs were polyreactive (*9*). In contrast, it was recently reported that one of three mAbs encoded by IGHV3-53, with limited somatic mutations (1.4%), reacted with the Ebola glycoprotein and HIV-1 gp140, and one of the four nAbs encoded by IGHV3-66 with limited somatic mutations (0.3%) showed moderate autoreactivity (*23*). Based on these observations, it is likely that auto- and polyreactivity may depend on specific somatic mutations and HCDR3 sequences.

We analyzed a possible correlation between clinical features and antibody responses of 17 individuals who were infected with SARS-CoV-2. Of 17 laboratory-confirmed patients, two patients (Patients M and O) had a severe respiratory illness that required mechanical ventilation and six patients (Patients A, H, I, K, L, and P) with moderate illness required supplemental oxygenation. These eight patients with relatively severe clinical courses had high titers of IgG antibody against SARS-CoV-2. However, three patients (Patients E, J, and Q) with mild/moderate symptoms also showed elevated titers of IgG antibody. Therefore, it is not clear whether antibody titers correlate with the clinical progression of the patients. Several reports describe a positive correlation between clinical severity and antibody titers (*24*, *25*), whereas a

contradictory report suggests that early seroconversion along with high antibody titers correlate with a less severe clinical course (*26*). In addition, there was a report claiming no association between comorbidity and antibody titer (*27*).

SARS-CoV-2 can cause a severe respiratory infection, which suggests that patients will need to produce both systemic and mucosal nAbs, including those of the IgA isotype, for protective immunity. Our results showed that IGHV3-53/IGHV3-66 and IGHJ6 class-switched to IgA_1 in Patients G, I, and J, and class-switched to IgA_1 and IgA_2 in Patient E (Table S3). After 99 days from the onset of symptoms, we did not detect any RBD-reactive IGH clonotypes in the peripheral blood of Patient E; however, the antibody titer to RBD remained high (Fig. 3D and Fig. 1). This observation is in line with the findings that nAb titers remain detectable among a fraction of SARS and MERS patients 1–2 years after infection (*28*, *29*). Therefore, it can be inferred that nAb-producing plasmablasts may be mobilized from the peripheral blood to bone marrow niches and continue to produce nAbs in Patient E. In these niches, plasmablasts are able to differentiate into mature Ab-secreting plasma cells and can survive for decades (*30*).

In the rhesus macaque model of SARS-CoV-2 infection, viral rechallenge generated a greater nAb titer than induced by primary infection and protected animals from reinfection (*31*). A single case of SARS-CoV-2 reinfection that has been reported suggests that it is possible for humans to become infected multiple times by SARS-CoV-2 (*32*). It is still unclear whether a SARS-CoV-2 vaccine would provide prolonged protective immunity to humans. The long-term production of nAbs, as seen in Patient E out to day 99 after symptom onset, suggests that nAb production by plasma cells in bone marrow niches may be a critical mechanism triggered by infection or vaccination that leads to protective immunity against SARS-CoV-2.

It has been reported that the frequency of RBD-reactive B cell clones is extremely low (0.07% to 0.005%) among circulating B cells (*24*). In our study, the frequency of isolated nAb clonotypes in the IGH repertoire was also extremely low (0.0004%-0.0064%), and Patient A had only one out of six nAbs that mapped to the IGH repertoire (Fig. 2B). As the complexity of scFv phage-display libraries exceeded 3.8×10^8 and 6.7×10^8 colony-forming units for Patient A, diverse RBD-binding clones could be enriched by biopanning. Only 199,561 unique IGH sequences were sampled by NGS in Patient A, whereas 515,994 IGH sequences were sampled in Patient E, when scFv phage-display libraries were constructed. This difference in NGS throughput might explain the discrepant allocation of nAb clonotypes in the IGH repertoire of Patients A and E. Consistent with this hypothesis, only 38.3% and 22.0% of "bind" and "predicted" clones were mapped for Patient A, respectively, whereas 77.8% and 32.1% of "bind" and "predicted" clones were individually mapped for Patient E.

A major limitation of this study was the limited number of patients enrolled made it difficult to analyze whether these stereotypic nAb clonotypes affect the clinical course of COVID-19. We found that stereotypic nAb clonotypes pre-existed in the majority of the naïve population, were prevalent among the patients who displayed rapid class-switching to IgG and IgA isotypes, and exhibited light chain plasticity among the SARS-CoV-2 RBD-binding antibodies. These results suggest that stereotypic nAb clonotypes may contribute to a milder clinical course and lower mortality rate in SARS-CoV-2 patients compared with SARS-CoV (9.5%) or MERS-CoV (34.4%) patients (*33*), for which similar stereotypic nAb clonotypes have not yet been reported. Future chronological follow-ups of Ig repertoires in a larger population of SARS-CoV-2 patients may provide insight into the effects of stereotypic nAb clonotypes on patient outcomes. Furthermore, studies assessing changes in the Ig repertoire among the naïve populations after SARS-CoV-2 vaccination may provide details about the contribution of these stereotypic nAb clonotypes to protective immunity.

MATERIALS AND METHODS

Study design

This study was designed to investigate stereotypic nAb clonotypes of SARS-CoV-2. 26 blood samples were collected from 17 SARS-CoV-2-positive patients and were subjected to NGS analysis of Ig sequences. Human antibody libraries were prepared and subjected to biopanning against recombinant SARS-CoV-2 RBD proteins. RBD-binders were selected using ELISA and their neutralization activity was tested using flow cytometry with ACE2-expressing Vero cells and recombinant SARS-CoV-2 S protein and microneutralization assay. NGS analysis of the enrichment patterns of clones through biopanning was performed for *in silico* selection of RBD-binding clones. Ig repertoire analyses were conducted to identify and characterize nAb clonotypes, including their prevalence among patients, frequency in Ig repertoires, somatic mutations, isotypes, chronological changes, and existence in a naïve uninfected population.

Clinical protocol and blood sample collection

All patients were confirmed to be infected by SARS-CoV-2 by a positive reverse transcriptase-quantitative polymerase chain reaction (RT-qPCR) result, and sample collection was performed at Seoul National University Hospital. The study involving human sample collection was approved by the Institutional Ethics Review Board of Seoul National University Hospital (IRB approval number: 2004-230-1119). Three chronological peripheral blood samples were drawn from Patients A and E, and two chronological samples were obtained from Patients B, C, D, F, and G. A single blood sample was collected from Patients H-Q. PBMCs and plasma were isolated using Lymphoprep (Stemcell Technologies, Vancouver,

BC, Canada), according to the manufacturer's protocol. PBMCs were subjected to total RNA isolation, using the TRI Reagent (Invitrogen, Carlsbad, CA, USA), according to the manufacturer's protocol.

Next-generation sequencing (NGS)

Genes encoding V_H and part of the CH1 domain were amplified, using specific primers, as described previously (*16*, *34*). All primers used are listed in Table S8. Briefly, total RNA was used as a template to synthesize cDNA, using the Superscript IV First-Strand Synthesis System (Invitrogen), with specific primers targeting the constant region (CH1 domain) of each isotype (IgM, IgD, IgG, IgA, and IgE) (*34*), according to the manufacturer's protocol. Following cDNA synthesis, 1.8 volumes of SPRI beads (AmpureXP, Beckman Coulter, Brea, CA, USA) were used to purify cDNA, which was eluted in 40 μL water. The purified cDNA (18 μL) was subjected to second-strand synthesis in a 25-μL reaction volume, using V gene-specific primers (*16*) and KAPA Biosystems (KAPA HiFi HotStart, Roche, Basel, Switzerland). The PCR conditions were as follows: 95°C for 3 min, 98°C for 1 min, 55°C for 1 min, and 72°C for 5 min. Following the second-strand synthesis, double-strand DNA (dsDNA) was purified, using SPRI beads, as described above. V_H genes were amplified using 15 μL eluted dsDNA and 2.5 pmol of the primers listed in Table S8, in a 50-μL total reaction volume (KAPA Biosystems), using the following thermal cycling program: 95°C for 3 min; 17 cycles of 98°C for 30 s, 65°C for 30 s, and 72°C for 1 min 10 s; and 72°C for 5 min. The number of PCR cycles was increased, from 17 to 19, for samples from Patients B (d10 and 19), C (d6), E (d23), and G (d9 and 22). PCR products were purified using SPRI beads and eluted in 30 μL water. Genes encoding V_κ and V_λ were amplified using specific primers, as described previously (*20*, *35*). Briefly, total RNA was used as a template to synthesize cDNA, using the Superscript IV First-Strand Synthesis System (Invitrogen), with specific primers targeting the constant region, which are listed in Table S8, according to the manufacturer's protocol. Following cDNA synthesis, SPRI beads were used to purify cDNA, which was eluted in 40 μL water. Purified cDNA (18 μL) was used for the first amplification, in a 25-μL reaction volume, using VJ gene-specific primers, which are listed in Table S8, and KAPA Biosystems. The PCR conditions were as follows: 95°C for 3 min, 4 cycles of 98°C for 1 min, 55°C for 1 min, and 72°C for 1 min; and 72°C for 10 min. Subsequently, DNA was purified using SPRI beads, and the V_κ and V_λ genes were amplified using 15 μL eluted dsDNA and 2.5 pmol of the primers listed in Table S8, in a 50-μL total reaction volume (KAPA Biosystems). The PCR conditions were as follows: 95°C for 3 min; 17 cycles of 98°C for 30 s, 65°C for 30 s, and 72°C for 1 min 10 s; and 72°C for 5 min. PCR products were purified using SPRI beads, as described above. For the amplification of V_H from each round of biopanning (rounds 0–4), gene fragments were amplified from phagemid DNA, using the primers listed in Table S8. SPRI-purified sequencing libraries were quantified with a 4200 TapeStation System (Agilent Technologies), using a D1000 ScreenTape Assay, before performing sequencing on an Illumina MiSeq Platform.

NGS data processing

Pre-processing of the NGS data for the IG repertoire

The raw NGS forward (R1) and reverse (R2) reads were merged by PEAR, v0.9.10, in default setting (*36*). The merged reads were q-filtered using the condition q20p95, which results in 95% of the base-pairs in a read having Phread scores higher than 20. The location of the primers was recognized from the q-filtered reads while allowing one substitution or deletion (Table S8). Primer regions that specifically bind to the molecules were trimmed in the reads to eliminate the effects of primer synthesis errors. Based on the primer recognition results, unique molecular identifier (UMI) sequences were extracted, and the reads were clustered according to the UMI sequences. To eliminate the possibility that the same UMI sequences might be used for different read amplifications, the clustered reads were subclustered, according to the similarity of the reads (Five mismatches were allowed in each subcluster). The subclustered reads were aligned using a multiple sequence alignment tool, Clustal Omega, v1.2.4, in default setting (*37*, *38*). From the aligned reads, the frequency of each nucleotide was calculated, and a consensus sequence of each subcluster was defined using the frequency information. The read count of the consensus sequence was redefined as the number of UMI subclusters that belong to the consensus sequences.

Sequence annotation, functionality filtering, and throughput adjustment

Sequence annotation consisted of two parts: isotype annotation and VDJ annotation. For annotation, the consensus sequence was divided into two sections, a VDJ region and a constant region, in a location-based manner. For isotype annotation, the extracted constant region was aligned with the IMGT (International Immunogenetics Information System) constant gene database (*39*). Based on the alignment results, the isotypes of the consensus sequences were annotated. Then, the VDJ regions of the consensus sequences were annotated using IgBLAST, v1.8.0 (*40*). Among the annotation results, V/D/J genes (V/J genes for V_L), CDR1/2/3 sequences, and the number of mutations from the corresponding V genes were extracted for further analysis. Divergence values were defined as the number of mutations identified in the aligned V gene, divided by the aligned length. The non-functional consensus reads were defined using the following criteria and filtered-out: 1. sequence length shorter than 250 bp; 2. existence of stop-codon or frame-shift in the full amino acid sequence; 3. annotation failure in one or more of the CDR1/2/3 regions; and 4. isotype annotation failure. The

functional consensus reads were random-sampled, to adjust the throughput of the V_H data (Table S5). Throughput adjustment was not conducted for V_L data (Table S6).

Preprocessing of the biopanning NGS data

Pre-processing of the biopanning NGS data was performed as previously reported, except for the application of the q-filtering condition q20p95 instead of q20p100 (*41*).

Overlapping IGH repertoire construction

To investigate the shared IGH sequences among the patients, we defined the overlapping IGH repertoire of the patients. Histograms for the nearest-neighbor distances of the HCDR3 amino acid sequences were calculated for the repertoire data. A hierarchical, distance-based analysis, which was reported previously (*42*), was applied to the HCDR3 amino acid sequences, to cluster functionally similar IGH sequences. The IGH sequences for all repertoire data could be approximated into a bimodal distribution, allowing the functionally similar IGH sequences to be extracted by capturing the first peak of the distribution (Figure S11). Threshold values for each data set were defined as the nearest-neighbor distance value of those points with a minimum frequency between the two peaks of the distribution. Then, the minimum value among all threshold values, 0.113871, was used to construct the overlapping IGH repertoire, which means that 11.3871% of mismatches in the HCDR3 amino acid sequence were allowed in the overlapping IGH repertoire construction. To construct the overlapping IGH repertoire, the repertoire data sets of all patients were merged into one data set. The IGH sequences in the merged data set were then clustered, using the following conditions: 1. the same V and J gene usage; and 2. mismatch smaller than 11.3871% among the HCDR3 amino acid sequences. Subsequently, clusters containing IGH sequences from more than one patient were included in the overlapping IGH repertoire data set.

Extraction of binding-predicted clones

From each round of biopanning (rounds 0, 2, 3, and 4), the V_H genes were amplified and subjected to NGS analysis, using the MiSeq platform, as described previously (*19*). Binding-predicted clones from biopanning were selected by analyzing the enrichment or diminishment patterns of clones in the NGS data from four libraries, A_d17, A_d45, E_d23, and E_d44, at each round of biopanning. The enrichment of clones primarily occurred during the second round of biopanning based on the input/output virus titer values for each round of biopanning and the frequencies of the clones in the NGS data (Figure S12). The frequency information in the NGS data sets for biopanning rounds 0, 2, 3, and 4 was subject to principal component analysis (PCA) for dimension reduction. Accordingly, principal component (PC)1 and PC2, which represented clone enrichment and clone depletion, respectively, were extracted. In the biopanning data, PC1 was primarily composed of the frequencies in rounds 2, 3, and 4, whereas PC2 was primarily composed of the frequency in round 0 (Figure S13). Thus, we defined PC1-major clones as the predicted clones, by setting constant threshold values on the PC1 value and the ratio between PC1 and PC2 (Table S7). 94.74% of the RBD-binding clones were mapped to the predicted clones (Figure S13).

Construction of a human scFv phage-display library and V_L shuffled libraries

For the V_H gene, the cDNA prepared for the NGS analysis was used. For the V_κ and V_λ genes, total RNA was used to synthesize cDNA, using the Superscript IV First-Strand Synthesis System (Invitrogen), with oligo(dT) primers, according to the manufacturer's instructions. Then, the genes encoding V_κ/V_λ and V_H were amplified, from the oligo(dT)-synthesized cDNA and the cDNA prepared for NGS analysis, respectively, using the primers listed in Table S8 and KAPA Biosystems. The PCR conditions were as follows: preliminary denaturation at 95°C for 3 min; 4 cycles of 98°C for 1 min, 55°C for 1 min, and 72°C for 1 min; and 72°C for 10 min. Subsequently, DNA was purified using SPRI beads, as described above. The purified DNA was amplified using the primers listed in Table S8 and KAPA Biosystems. The PCR conditions were as follows: preliminary denaturation, at 95°C for 3 min; 25 cycles of 98°C for 30 s, 58°C for 30 s, and 72°C for 90 s; and 72°C for 10 min. Then, the V_H and V_κ/V_λ fragments were subjected to electrophoresis, on a 1% agarose gel, and purified, using a QIAquick Gel Extraction Kit (Qiagen Inc., Valencia, CA, USA), according to the manufacturer's instructions. The purified V_H and V_κ/V_λ fragments were mixed, at equal ratios at 50 ng, and subjected to overlap extension, to generate scFv genes, using the primers listed in Table S8 and KAPA Biosystems. The PCR conditions were as follows: preliminary denaturation, at 94°C for 5 min; 25 cycles of 98°C for 15 s, 56°C for 15 s, and 72°C for 2 min; and 72°C for 10 min. The amplified scFv fragment was purified and cloned into a phagemid vector, as described previously (*43*).

For the construction of V_κ/V_λ shuffled libraries, gBlocks Gene Fragments (Integrated DNA Technologies, Coralville, IA, USA), encoding A-11, E-12, A-31, A-32, B-33, E-34, A,B,G-42, G-44, D-51, F-53, E-52, and A-54, were synthesized. Synthesized V_H and the V_κ/V_λ genes from Patients A, E, and G were used to synthesize the scFv libraries using PCR, as described previously (*43*). Then, the amplified scFv fragments were purified and cloned into the phagemid vector, as described above.

Biopanning

Phage display of the human scFv libraries exceeded complexity of 3.8×10^8, 6.7×10^8, 2.0×10^8, and 7.2×10^8 colony-forming units for A_d17, A_d45, E_d23, and E_d44, respectively. These libraries were subjected to four rounds of biopanning against the recombinant SARS-CoV-2 RBD protein (Sino Biological Inc., Beijing, China), fused to mFc or hC_κ, as

described previously (*44*). Briefly, 3 μg of the recombinant SARS-CoV-2 RBD protein was conjugated to 1.0×10^7 magnetic beads (Dynabeads M-270 epoxy, Invitrogen) and incubated with the scFv phage-display libraries (approximately 10^{12} phages), for 2 hours at 37°C. During the first round of biopanning, the beads were washed once with 500 μL of 0.05% (v/v) Tween-20 (Sigma-Aldrich, St. Louis, MO, USA) in phosphate-buffered saline (PBST). For the other rounds of biopanning, 1.5 μg of recombinant SARS-CoV-2 RBD protein was conjugated to 5.0×10^6 magnetic beads, and the number of washes was increased to three. After each round of biopanning, the bound phages were eluted and rescued, as described previously (*44*).

Phage ELISA

To select SARS-CoV-2 S reactive clones, phage ELISA was performed, using recombinant S and RBD protein-coated microtiter plates, as described previously (*45*). Reactive scFv clones were subjected to Sanger sequencing (Cosmogenetech, Seoul, Republic of Korea), to determine their nucleotide sequences.

Expression of recombinant proteins

A human, codon-optimized, SARS-CoV-2 RBD (YP_009724390.1, amino acids 306–543) gene was synthesized (Integrated DNA Technologies). Using a synthesized wild-type RBD gene as a template, RBD mutants (V341I, F342L, N354D, N354D/D364Y, V367F, R408I, A435S, W436R, G476S, and V483A) were generated through two-step PCR, using the primers listed in Table S8. The genes encoding wild-type or mutant SARS-CoV-2 RBD were cloned into a modified mammalian expression vector, containing the hC_K gene (*44*), and transfected into Expi293F (Invitrogen) cells. The fusion proteins were purified by affinity chromatography, using KappaSelect Columns (GE Healthcare, Chicago, IL, USA), as described previously (*46*). Due to low expression yields, two RBD mutants (N354D/D364Y, W436R) were excluded from further studies.

The genes encoding the selected scFv clones were cloned into a modified mammalian expression vector, containing the $hIgG_1$ Fc regions (hFc) or hC_K at the C terminus (*44*, *47*), before being transfected and purified by affinity chromatography, as described above.

Genes encoding V_H and V_L were amplified, cloned into a mammalian expression vector containing the CH1 and hinge regions of human IgG_2 fused to the CH2 and CH3 regions of human IgG_4 (*48*, *49*), and transfected into Expi293F cells (Invitrogen) as described previously (*50*). Then, IgG2/4 was purified by affinity chromatography using MabSelect columns with the AKTA Pure chromatography system (GE Healthcare) following the manufacturer's protocol.

ELISA

100 ng of each recombinant SARS-CoV-2 S (Sino Biological Inc.), S1 (Sino Biological Inc.), S1 D614G (Sino Biological Inc.), S2 (Sino Biological Inc.), NP (Sino Biological Inc.), RBD, RBD mutants, SARS-CoV RBD (Sino Biological Inc.), MERS-CoV S (Sino Biological Inc.), RBD (Sino Biological Inc.), S2 (Sino Biological Inc.) proteins were added to microtiter plates (Costar), in coating buffer (0.1 M sodium bicarbonate, pH 8.6). After incubation at 4°C, overnight and blocking with 3% bovine serum albumin (BSA) in PBS, for 1 hour at 37°C, serially diluted plasma (5-fold, 6 dilutions, starting from 1:100) or scFv-hFc (5-fold, 12 dilutions, starting from 1,000 or 500 nM) in blocking buffer was added to individual wells and incubated for 1, h at 37°C. Then, plates were washed three times with 0.05% PBST. Horseradish peroxidase (HRP)-conjugated rabbit anti-human IgG antibody (Invitrogen) or anti-human Ig kappa light chain antibody (Millipore, Temecula, CA, USA), in blocking buffer (1:5,000), was added to wells and incubated for 1 hour at 37°C. After washing three times with PBST, 2,2′-azino-bis-3-ethylbenzothiazoline-6-sulfonic (ThermoFisher Scientific Inc., Waltham, MA, USA) or 3,3′,5,5′-Tetramethylbenzidine liquid substrate system (ThermoFisher Scientific Inc.) was added to the wells. Absorbance was measured at 405 nm or 650 nm, respectively, using a microplate spectrophotometer (Multiskan GO; Thermo Scientific).

Flow cytometry

The recombinant SARS-CoV-2 S protein (200 nM), fused with a HIS-tag at the C terminus (Sino Biological Inc.), was incubated with scFv-hFc fusion proteins at a final concentration of either 200 nM (equimolar) or 600 nM (molar ratio of 1:3), in 50 μL of 1% (w/v) BSA in PBS, containing 0.02% (w/v) sodium azide (FACS buffer), at 37°C for 1 hour. Irrelevant scFv-hFc or scFv-hC_K fusion proteins were used as negative controls. Vero E6 cells ($ACE2^+$) were seeded into v-bottom 96-well plates (Corning, Corning, NY, USA), at a density of 1.5×10^5 cells per well. Then, the mixture was added to each well and incubated, at 37°C for 1 hour. After washing three times with FACS buffer, FITC-labeled rabbit anti-HIS Ab (Abcam, Cambridge, UK) was incubated, at 37°C for 1 hour. Then, the cells were washed three times with FACS buffer, resuspended in 150 μL of PBS, and subjected to analysis by flow cytometry, using a FACS Canto II instrument (BD Bioscience, San Jose, CA, USA). For each sample, 10,000 cells were analyzed.

Microneutralization assay

The virus (BetaCoV/Korea/SNU01/2020, accession number MT039890) was isolated at the Seoul National University Hospital and propagated in Vero cells (ATCC CCL-81), using Dulbecco's Modified Eagle's Medium (DMEM, Welgene, Gyeongsan, Republic of Korea) supplemented with 2% fetal bovine serum (Gibco) (*51*). The cells were grown in T-25 flasks, (ThermoFisher Scientific Inc.), inoculated with SARS-CoV-2, and incubated at 37°C, in a 5% CO_2 environment. 3 days after inoculation, virus was harvested from culture supernatants and stored at -80°C. The virus titer was

determined via a $TCID_{50}$ assay (*52*).

Vero cells were seeded in T-25 flasks and grown for 24 hours, at 37°C, in a 5% CO_2 environment, to ensure 80% confluency on the day of inoculation. The recombinant scFv-hCκ fusion proteins (0.5, 5, or 50 μg/mL) were mixed with 2,500 $TCID_{50}$ of SARS-CoV-2, and the mixture was incubated for 2 hours, at 37°C. The mixture (1 mL) was added to Vero cells and incubated for 1 hour, at 37°C, in a 5% CO_2 environment. After incubation for 1 hour, 6 mL of complete media was added to the flasks and incubated, at 37°C, in a 5% CO_2 environment. After 0, 24, 48, and 72 hours of infection, the culture supernatant was collected, to measure the virus titers. Viral RNA was extracted using the MagNA Pure 96 DNA and Viral NA small volume kit (Roche, Germany), according to the manufacturer's instructions. Viral RNA was detected using the PowerChek 2019-nCoV Real-time PCR Kit (Kogene Biotech, Seoul, Republic of Korea), for the amplification of the E gene and quantified according to a standard curve, which was constructed using in vitro transcribed RNA provided by the European Virus Archive (https://www.european-virus-archive.com). An alternative neutralization assay was performed as described previously (*53*). Briefly, Vero cells were seeded in 96-well flat-bottom tissue culture microtiter plates in DMEM medium were grown for 24 hours at 37°C in a 5% CO_2 environment. 50 μl of two-fold serially diluted IgG2/4 were mixed with an equal volume of SARS-CoV-2 containing 100 $TCID_{50}$ and the IgG2/4-virus mixture was incubated at 37 °C for 1 hour. The mixture was then transferred into a 96-well microtiter plate containing Vero cells with 8 repeats and incubated for 5 days at 37°C in a 5% CO_2 environment. Cells infected with 100 $TCID_{50}$ of SARS-CoV-2, isotype IgG2/4 control, or without the virus, were applied as positive, negative, and uninfected controls, respectively. The cytopathic effect (CPE) in each well was observed 5 days post-infection. The IC_{50} was calculated using GraphPad Prism 8 (GraphPad Software, San Diego, CA, USA). All experiments using authentic SARS-CoV-2 were conducted in Biosafety Level 3 laboratory.

Statistical analyses

Data are represented as mean ± standard deviation. Statistical analyses were performed using R software v.3.4.3. For the flow cytometry analysis using ACE2-expressing cells and recombinant SARS-CoV-2 S protein, results were analyzed by independent *t*-tests.

SUPPLEMENTARY MATERIALS

stm.sciencemag.org/cgi/content/full/scitranslmed.abd6990/DC1

Fig. S1. Titrations of serum IgG by ELISAs specific to MERS-CoV.
Fig. S2. Reactivity of anti-SARS-CoV-2 scFv antibodies against recombinant SARS-CoV-2 RBD
Fig. S3. Inhibition of recombinant SARS-CoV-2 S glycoprotein binding to ACE2-expressing cells.
Fig. S4. In vitro neutralization of SARS-COV-2.
Fig. S5. Mapping of 11 nAbs to the overlapping IGH repertoire.
Fig. S6. Existence of V_L that can be paired with the stereotypic V_H.
Fig. S7. VJ gene usage among the IG kappa light chain repertoire of patients.
Fig. S8. VJ gene usage among the IG lambda light chain repertoire of patients.
Fig. S9. Reactivity of phage-displayed scFv clones in phage ELISA.
Fig. S10. Deep profiling of the IGH repertoire of Patients B, C, D, F, and G.
Fig. S11. The nearest-neighbor distance histogram for HCDR3 amino acid sequences in the IGH repertoires of patients.
Fig. S12. Frequency scatter plots for NGS data from four libraries after each round of biopanning.
Fig. S13. The results of principal component analysis (PCA) applied to the NGS data of four libraries after each round of biopanning.
Table S1. Demographic and clinical characteristics.
Table S2. SARS-CoV-2 RBD-reactive scFv clones.
Table S3. Class-switched IGH clonotypes homologous to E-3B1.
Table S4. Human mAbs reactive against MERS-CoV RBD.
Table S5. Statistics for the pre-processing of the IGH NGS data.
Table S6. Statistics for the pre-processing of the IGκ and IGλ NGS data.
Table S7. The RBD-binding prediction clones.
Table S8. Primers used in the study.
Data file S1. Individual level data.

REFERENCES AND NOTES

1. J. G. Jardine, T. Ota, D. Sok, M. Pauthner, D. W. Kulp, O. Kalyuzhniy, P. D. Skog, T. C. Thinnes, D. Bhullar, B. Briney, S. Menis, M. Jones, M. Kubitz, S. Spencer, Y. Adachi, D. R. Burton, W. R. Schief, D. Nemazee, HIV-1 VACCINES. Priming a broadly neutralizing antibody response to HIV-1 using a germline-targeting immunogen. *Science* **349**, 156–161 (2015). doi:10.1126/science.aac5894 Medline
2. J. R. Willis, J. A. Finn, B. Briney, G. Sapparapu, V. Singh, H. King, C. C. LaBranche, D. C. Montefiori, J. Meiler, J. E. Crowe Jr., Long antibody HCDR3s from HIV-naïve donors presented on a PG9 neutralizing antibody background mediate HIV neutralization. *Proc. Natl. Acad. Sci. U.S.A.* **113**, 4446–4451 (2016). doi:10.1073/pnas.1518405113 Medline
3. N. Eroshenko, T. Gill, M. K. Keaveney, G. M. Church, J. M. Trevejo, H. Rajaniemi, Implications of antibody-dependent enhancement of infection for SARS-CoV-2 countermeasures. *Nat. Biotechnol.* **38**, 789–791 (2020). doi:10.1038/s41587-020-0577-1 Medline
4. A. Iwasaki, Y. Yang, The potential danger of suboptimal antibody responses in COVID-19. *Nat. Rev. Immunol.* **20**, 339–341 (2020). doi:10.1038/s41577-020-0321-6 Medline
5. M. K. Smatti, A. A. Al Thani, H. M. Yassine, Viral-Induced Enhanced Disease Illness. *Front. Microbiol.* **9**, 2991 (2018). doi:10.3389/fmicb.2018.02991 Medline
6. A. Zhang, H. D. Stacey, C. E. Mullarkey, M. S. Miller, Original Antigenic Sin: How First Exposure Shapes Lifelong Anti-Influenza Virus Immune Responses. *J. Immunol.* **202**, 335–340 (2019). doi:10.4049/jimmunol.1801149 Medline
7. Y. Cao, B. Su, X. Guo, W. Sun, Y. Deng, L. Bao, Q. Zhu, X. Zhang, Y. Zheng, C. Geng, X. Chai, R. He, X. Li, Q. Lv, H. Zhu, W. Deng, Y. Xu, Y. Wang, L. Qiao, Y. Tan, L. Song, G. Wang, X. Du, N. Gao, J. Liu, J. Xiao, X. D. Su, Z. Du, Y. Feng, C. Qin, C. Qin, R. Jin, X. S. Xie, Potent neutralizing antibodies against SARS-CoV-2 identified by high-throughput single-cell sequencing of convalescent patients' B cells. *Cell* **182**, 73–84.e16 (2020). doi:10.1016/j.cell.2020.05.025 Medline
8. B. Ju, Q. Zhang, J. Ge, R. Wang, J. Sun, X. Ge, J. Yu, S. Shan, B. Zhou, S. Song, X. Tang, J. Yu, J. Lan, J. Yuan, H. Wang, J. Zhao, S. Zhang, Y. Wang, X. Shi, L. Liu, J. Zhao, X. Wang, Z. Zhang, L. Zhang, Human neutralizing antibodies elicited by SARS-CoV-2 infection. *Nature* **584**, 115–119 (2020). doi:10.1038/s41586-020-2380-z Medline
9. T. F. Rogers, F. Zhao, D. Huang, N. Beutler, A. Burns, W. T. He, O. Limbo, C. Smith, G. Song, J. Woehl, L. Yang, R. K. Abbott, S. Callaghan, E. Garcia, J. Hurtado, M. Parren, L. Peng, S. Ramirez, J. Ricketts, M. J. Ricciardi, S. A. Rawlings, N. C. Wu, M. Yuan, D. M. Smith, D. Nemazee, J. R. Teijaro, J. E. Voss, I. A. Wilson, R. Andrabi, B. Briney, E. Landais, D. Sok, J. G. Jardine, D. R. Burton, Isolation of potent SARS-CoV-2 neutralizing antibodies and protection from disease in a small animal model. *Science* **369**, 956–963 (2020). doi:10.1126/science.abc7520 Medline
10. R. Shi, C. Shan, X. Duan, Z. Chen, P. Liu, J. Song, T. Song, X. Bi, C. Han, L. Wu, G. Gao, X. Hu, Y. Zhang, Z. Tong, W. Huang, W. J. Liu, G. Wu, B. Zhang, L. Wang, J. Qi, H. Feng, F. S. Wang, Q. Wang, G. F. Gao, Z. Yuan, J. Yan, A human neutralizing antibody targets the receptor-binding site of SARS-CoV-2. *Nature* **584**, 120–124 (2020). doi:10.1038/s41586-020-2381-y Medline

11. Y. Wu, F. Wang, C. Shen, W. Peng, D. Li, C. Zhao, Z. Li, S. Li, Y. Bi, Y. Yang, Y. Gong, H. Xiao, Z. Fan, S. Tan, G. Wu, W. Tan, X. Lu, C. Fan, Q. Wang, Y. Liu, C. Zhang, J. Qi, G. F. Gao, F. Gao, L. Liu, A noncompeting pair of human neutralizing antibodies block COVID-19 virus binding to its receptor ACE2. *Science* **368**, 1274–1278 (2020). doi:10.1126/science.abc2241 Medline
12. M. Yuan, H. Liu, N. C. Wu, C. D. Lee, X. Zhu, F. Zhao, D. Huang, W. Yu, Y. Hua, H. Tien, T. F. Rogers, E. Landais, D. Sok, J. G. Jardine, D. R. Burton, I. A. Wilson, Structural basis of a shared antibody response to SARS-CoV-2. *Science* **369**, 1119–1123 (2020). doi:10.1126/science.abd2321 Medline
13. D. Wrapp, N. Wang, K. S. Corbett, J. A. Goldsmith, C. L. Hsieh, O. Abiona, B. S. Graham, J. S. McLellan, Cryo-EM structure of the 2019-nCoV spike in the prefusion conformation. *Science* **367**, 1260–1263 (2020). doi:10.1126/science.abb2507 Medline
14. Q. Wang, Y. Zhang, L. Wu, S. Niu, C. Song, Z. Zhang, G. Lu, C. Qiao, Y. Hu, K. Y. Yuen, Q. Wang, H. Zhou, J. Yan, J. Qi, Structural and Functional Basis of SARS-CoV-2 Entry by Using Human ACE2. *Cell* **181**, 894–904.e9 (2020). doi:10.1016/j.cell.2020.03.045 Medline
15. P. Zhou, X. L. Yang, X. G. Wang, B. Hu, L. Zhang, W. Zhang, H. R. Si, Y. Zhu, B. Li, C. L. Huang, H. D. Chen, J. Chen, Y. Luo, H. Guo, R. D. Jiang, M. Q. Liu, Y. Chen, X. R. Shen, X. Wang, X. S. Zheng, K. Zhao, Q. J. Chen, F. Deng, L. L. Liu, B. Yan, F. X. Zhan, Y. Y. Wang, G. F. Xiao, Z. L. Shi, A pneumonia outbreak associated with a new coronavirus of probable bat origin. *Nature* **579**, 270–273 (2020). doi:10.1038/s41586-020-2012-7 Medline
16. B. Briney, A. Inderbitzin, C. Joyce, D. R. Burton, Commonality despite exceptional diversity in the baseline human antibody repertoire. *Nature* **566**, 393–397 (2019). doi:10.1038/s41586-019-0879-y Medline
17. S. I. Kim, S. Kim, J. Kim, S. Y. Chang, J. M. Shim, J. Jin, C. Lim, S. Baek, J. Y. Min, W. B. Park, M. D. Oh, S. Kim, J. Chung, Generation of a Nebulizable CDR-Modified MERS-CoV Neutralizing Human Antibody. *Int. J. Mol. Sci.* **20**, 5073 (2019). doi:10.3390/ijms20205073 Medline
18. W. Yang, A. Yoon, S. Lee, S. Kim, J. Han, J. Chung, Next-generation sequencing enables the discovery of more diverse positive clones from a phage-displayed antibody library. *Exp. Mol. Med.* **49**, e308 (2017). doi:10.1038/emm.2017.22 Medline
19. D. K. Yoo, S. R. Lee, Y. Jung, H. Han, H. K. Lee, J. Han, S. Kim, J. Chae, T. Ryu, J. Chung, Machine Learning-Guided Prediction of Antigen-Reactive In Silico Clonotypes Based on Changes in Clonal Abundance through Bio-Panning. *Biomolecules* **10**, 421 (2020). doi:10.3390/biom10030421 Medline
20. C. Soto, R. G. Bombardi, A. Branchizio, N. Kose, P. Matta, A. M. Sevy, R. S. Sinkovits, P. Gilchuk, J. A. Finn, J. E. Crowe Jr., High frequency of shared clonotypes in human B cell receptor repertoires. *Nature* **566**, 398–402 (2019). doi:10.1038/s41586-019-0934-8 Medline
21. J. Ou, Z. Zhou, R. Dai, J. Zhang, W. Lan, S. Zhao, J. Wu, D. Seto, L. Cui, G. Zhang, Q. Zhang, Emergence of RBD mutations in circulating SARS-CoV-2 strains enhancing the structural stability and human ACE2 receptor affinity of the spike protein. *bioRxiv*, 2020.2003.2015.991844 (2020).
22. J. Kreye, S. M. Reincke, H.-C. Kornau, E. Sánchez-Sendin, V. Max Corman, H. Liu, M. Yuan, N. C. Wu, X. Zhu, C. D. Lee, J. Trimpert, M. Höltje, K. Dietert, L. Stöffler, N. von Wardenburg, S. van Hoof, M. A. Homeyer, J. Hoffmann, A. Abdelgawad, A. D. Gruber, L. D. Bertzbach, D. Vladimirova, L. Y. Li, P. C. Barthel, K. Skriner, A. C. Hocke, S. Hippenstiel, M. Witzenrath, N. Suttorp, F. Kurth, C. Franke, M. Endres, D. Schmitz, L. M. Jeworowski, A. Richter, M. L. Schmidt, T. Schwarz, M. A. Müller, C. Drosten, D. Wendisch, L. E. Sander, N. Osterrieder, I. A. Wilson, H. Prüss, A SARS-CoV-2 neutralizing antibody protects from lung pathology in a COVID-19 hamster model. *bioRxiv* 2020.2008.2015.252320 (2020). doi:10.2139/ssrn.3680870 Medline
23. C. Kreer, M. Zehner, T. Weber, M. S. Ercanoglu, L. Gieselmann, C. Rohde, S. Halwe, M. Korenkov, P. Schommers, K. Vanshylla, V. Di Cristanziano, H. Janicki, R. Brinker, A. Ashurov, V. Krähling, A. Kupke, H. Cohen-Dvashi, M. Koch, J. M. Eckert, S. Lederer, N. Pfeifer, T. Wolf, M. J. G. T. Vehreschild, C. Wendtner, R. Diskin, H. Gruell, S. Becker, F. Klein, Longitudinal Isolation of Potent Near-Germline SARS-CoV-2-Neutralizing Antibodies from COVID-19 Patients. *Cell* **182**, 843–854.e12 (2020). doi:10.1016/j.cell.2020.06.044 Medline
24. D. F. Robbiani, C. Gaebler, F. Muecksch, J. C. C. Lorenzi, Z. Wang, A. Cho, M. Agudelo, C. O. Barnes, A. Gazumyan, S. Finkin, T. Hägglöf, T. Y. Oliveira, C. Viant, A. Hurley, H. H. Hoffmann, K. G. Millard, R. G. Kost, M. Cipolla, K. Gordon, F. Bianchini, S. T. Chen, V. Ramos, R. Patel, J. Dizon, I. Shimeliovich, P. Mendoza, H. Hartweger, L. Nogueira, M. Pack, J. Horowitz, F. Schmidt, Y. Weisblum, E. Michailidis, A. W. Ashbrook, E. Waltari, J. E. Pak, K. E. Huey-Tubman, N. Koranda, P. R. Hoffman, A. P. West Jr., C. M. Rice, T. Hatziioannou, P. J. Bjorkman, P. D. Bieniasz, M. Caskey, M. C. Nussenzweig, Convergent antibody responses to SARS-CoV-2 in convalescent individuals. *Nature* **584**, 437–442 (2020). doi:10.1038/s41586-020-2456-9 Medline
25. J. Zhao, Q. Yuan, H. Wang, W. Liu, X. Liao, Y. Su, X. Wang, J. Yuan, T. Li, J. Li, S. Qian, C. Hong, F. Wang, Y. Liu, Z. Wang, Q. He, Z. Li, B. He, T. Zhang, Y. Fu, S. Ge, L. Liu, J. Zhang, N. Xia, Z. Zhang, Antibody responses to SARS-CoV-2 in patients with novel coronavirus disease 2019. *Clin. Infect. Dis.* **71**, 2027–2034 (2020). doi:10.1093/cid/ciaa344 Medline
26. W. H. Kong, R. Zhao, J. B. Zhou, F. Wang, D. G. Kong, J. B. Sun, Q. F. Ruan, M. Q. Liu, Serologic Response to SARS-CoV-2 in COVID-19 Patients with Different Severity. *Virol. Sin.* (2020). doi:10.1007/s12250-020-00270-x Medline
27. K. K. To, O. T. Tsang, W. S. Leung, A. R. Tam, T. C. Wu, D. C. Lung, C. C. Yip, J. P. Cai, J. M. Chan, T. S. Chik, D. P. Lau, C. Y. Choi, L. L. Chen, W. M. Chan, K. H. Chan, J. D. Ip, A. C. Ng, R. W. Poon, C. T. Luo, V. C. Cheng, J. F. Chan, I. F. Hung, Z. Chen, H. Chen, K. Y. Yuen, Temporal profiles of viral load in posterior oropharyngeal saliva samples and serum antibody responses during infection by SARS-CoV-2: An observational cohort study. *Lancet Infect. Dis.* **20**, 565–574 (2020). doi:10.1016/S1473-3099(20)30196-1 Medline
28. P. G. Choe, R. A. P. M. Perera, W. B. Park, K. H. Song, J. H. Bang, E. S. Kim, H. B. Kim, L. W. R. Ko, S. W. Park, N. J. Kim, E. H. Y. Lau, L. L. M. Poon, M. Peiris, M. D. Oh, MERS-CoV Antibody Responses 1 Year after Symptom Onset, South Korea, 2015. *Emerg. Infect. Dis.* **23**, 1079–1084 (2017). doi:10.3201/eid2307.170310 Medline
29. L. P. Wu, N. C. Wang, Y. H. Chang, X. Y. Tian, D. Y. Na, L. Y. Zhang, L. Zheng, T. Lan, L. F. Wang, G. D. Liang, Duration of antibody responses after severe acute respiratory syndrome. *Emerg. Infect. Dis.* **13**, 1562–1564 (2007). doi:10.3201/eid1310.070576 Medline
30. D. Tarlinton, A. Radbruch, F. Hiepe, T. Dörner, Plasma cell differentiation and survival. *Curr. Opin. Immunol.* **20**, 162–169 (2008). doi:10.1016/j.coi.2008.03.016 Medline
31. W. Deng, L. Bao, J. Liu, C. Xiao, J. Liu, J. Xue, Q. Lv, F. Qi, H. Gao, P. Yu, Y. Xu, Y. Qu, F. Li, Z. Xiang, H. Yu, S. Gong, M. Liu, G. Wang, S. Wang, Z. Song, Y. Liu, W. Zhao, Y. Han, L. Zhao, X. Liu, Q. Wei, C. Qin, Primary exposure to SARS-CoV-2 protects against reinfection in rhesus macaques. *Science* **369**, 818–823 (2020). doi:10.1126/science.abc5343 Medline
32. R. L. Tillett, J. R. Sevinsky, P. D. Hartley, H. Kerwin, N. Crawford, A. Gorzalski, C. Laverdure, S. C. Verma, C. C. Rossetto, D. Jackson, M. J. Farrell, S. V. Hooser, M. Pandori, Genomic evidence for reinfection with SARS-CoV-2: A case study. *Lancet Infect. Dis.* (2020). Medline
33. V. J. Munster, M. Koopmans, N. van Doremalen, D. van Riel, E. de Wit, A Novel Coronavirus Emerging in China - Key Questions for Impact Assessment. *N. Engl. J. Med.* **382**, 692–694 (2020). doi:10.1056/NEJMp2000929 Medline
34. F. Horns, C. Vollmers, D. Croote, S. F. Mackey, G. E. Swan, C. L. Dekker, M. M. Davis, S. R. Quake, Lineage tracing of human B cells reveals the in vivo landscape of human antibody class switching. *eLife* **5**, e16578 (2016). doi:10.7554/eLife.16578 Medline
35. H. Wardemann, S. Yurasov, A. Schaefer, J. W. Young, E. Meffre, M. C. Nussenzweig, Predominant autoantibody production by early human B cell precursors. *Science* **301**, 1374–1377 (2003). doi:10.1126/science.1086907 Medline
36. J. Zhang, K. Kobert, T. Flouri, A. Stamatakis, PEAR: A fast and accurate Illumina Paired-End reAd mergeR. *Bioinformatics* **30**, 614–620 (2014). doi:10.1093/bioinformatics/btt593 Medline
37. F. Sievers, D. G. Higgins, Clustal Omega for making accurate alignments of many protein sequences. *Protein Sci.* **27**, 135–145 (2018). doi:10.1002/pro.3290 Medline
38. F. Sievers, A. Wilm, D. Dineen, T. J. Gibson, K. Karplus, W. Li, R. Lopez, H. McWilliam, M. Remmert, J. Söding, J. D. Thompson, D. G. Higgins, Fast, scalable generation of high-quality protein multiple sequence alignments using Clustal Omega. *Mol. Syst. Biol.* **7**, 539 (2011). doi:10.1038/msb.2011.75 Medline
39. M. P. Lefranc, IMGT databases, web resources and tools for immunoglobulin and

T cell receptor sequence analysis, http://imgt.cines.fr. *Leukemia* **17**, 260–266 (2003). doi:10.1038/sj.leu.2402637 Medline
40. J. Ye, N. Ma, T. L. Madden, J. M. Ostell, IgBLAST: An immunoglobulin variable domain sequence analysis tool. *Nucleic Acids Res.* **41** (W1), W34-40 (2013). doi:10.1093/nar/gkt382 Medline
41. S. Kim, H. Lee, J. Noh, Y. Lee, H. Han, D. K. Yoo, H. Kim, S. Kwon, J. Chung, Efficient Selection of Antibodies Reactive to Homologous Epitopes on Human and Mouse Hepatocyte Growth Factors by Next-Generation Sequencing-Based Analysis of the B Cell Repertoire. *Int. J. Mol. Sci.* **20**, 417 (2019). doi:10.3390/ijms20020417 Medline
42. N. T. Gupta, K. D. Adams, A. W. Briggs, S. C. Timberlake, F. Vigneault, S. H. Kleinstein, Hierarchical Clustering Can Identify B Cell Clones with High Confidence in Ig Repertoire Sequencing Data. *J. Immunol.* **198**, 2489–2499 (2017). doi:10.4049/jimmunol.1601850 Medline
43. J. Andris-Widhopf, P. Steinberger, R. Fuller, C. Rader, C. F. Barbas 3rd, Generation of human scFv antibody libraries: PCR amplification and assembly of light- and heavy-chain coding sequences. *Cold Spring Harb. Protoc.* **2011**, pdb.prot065573 (2011). doi:10.1101/pdb.prot065573 Medline
44. Y. Lee, H. Kim, J. Chung, An antibody reactive to the Gly63-Lys68 epitope of NT-proBNP exhibits O-glycosylation-independent binding. *Exp. Mol. Med.* **46**, e114 (2014). doi:10.1038/emm.2014.57 Medline
45. F. Carlos Barbas III, D. R. Burton, J. K. Scott, G. J. Silverman, *Phage Display: A Laboratory Manual* (Cold Spring Harbor Laboratory Press, 2001), pp. 487-488.
46. S. Lee, I. H. Yoon, A. Yoon, J. M. Cook-Mills, C. G. Park, J. Chung, An antibody to the sixth Ig-like domain of VCAM-1 inhibits leukocyte transendothelial migration without affecting adhesion. *J. Immunol.* **189**, 4592–4601 (2012). doi:10.4049/jimmunol.1103803 Medline
47. S. Park, D. H. Lee, J. G. Park, Y. T. Lee, J. Chung, A sensitive enzyme immunoassay for measuring cotinine in passive smokers. *Clin. Chim. Acta* **411**, 1238–1242 (2010). doi:10.1016/j.cca.2010.04.027 Medline
48. J. P. Mueller, M. A. Giannoni, S. L. Hartman, E. A. Elliott, S. P. Squinto, L. A. Matis, M. J. Evans, Humanized porcine VCAM-specific monoclonal antibodies with chimeric IgG2/G4 constant regions block human leukocyte binding to porcine endothelial cells. *Mol. Immunol.* **34**, 441–452 (1997). doi:10.1016/S0161-5890(97)00042-4 Medline
49. R. P. Rother, S. A. Rollins, C. F. Mojcik, R. A. Brodsky, L. Bell, Discovery and development of the complement inhibitor eculizumab for the treatment of paroxysmal nocturnal hemoglobinuria. *Nat. Biotechnol.* **25**, 1256–1264 (2007). doi:10.1038/nbt1344 Medline
50. J. Jin, G. Park, J. B. Park, S. Kim, H. Kim, J. Chung, An anti-EGFR × cotinine bispecific antibody complexed with cotinine-conjugated duocarmycin inhibits growth of EGFR-positive cancer cells with KRAS mutations. *Exp. Mol. Med.* **50**, 1–14 (2018). doi:10.1038/s12276-018-0177-z Medline
51. W. B. Park, N. J. Kwon, S. J. Choi, C. K. Kang, P. G. Choe, J. Y. Kim, J. Yun, G. W. Lee, M. W. Seong, N. J. Kim, J. S. Seo, M. D. Oh, Virus Isolation from the First Patient with SARS-CoV-2 in Korea. *J. Korean Med. Sci.* **35**, e84 (2020). doi:10.3346/jkms.2020.35.e84 Medline
52. L. J. REED, H. MUENCH, A SIMPLE METHOD OF ESTIMATING FIFTY PER CENT ENDPOINTS12. *Am. J. Epidemiol.* **27**, 493–497 (1938). doi:10.1093/oxfordjournals.aje.a118408
53. R. Shi, C. Shan, X. Duan, Z. Chen, P. Liu, J. Song, T. Song, X. Bi, C. Han, L. Wu, G. Gao, X. Hu, Y. Zhang, Z. Tong, W. Huang, W. J. Liu, G. Wu, B. Zhang, L. Wang, J. Qi, H. Feng, F. S. Wang, Q. Wang, G. F. Gao, Z. Yuan, J. Yan, A human neutralizing antibody targets the receptor-binding site of SARS-CoV-2. *Nature* **584**, 120–124 (2020). doi:10.1038/s41586-020-2381-y Medline

Acknowledgments: The authors thank Su Jin Choi for technical support. **Funding:** This research was funded by the National Research Foundation of Korea [NRF-2016M3A9B6918973] and the Ministry of Science and ICT(MSIT) of the Republic of Korea and the National Research Foundation of Korea [NRF-2020R1A3B3079653]. This research was supported by the Global Research Development Center Program, through the NRF, funded by the MSIT [2015K1A4A3047345]. This work was supported by the Brain Korea 21 Plus Project in 2020. **Author contributions:** Sang Il K. designed and conducted all experiments, performed analyses, interpreted experimental results, wrote and revised the paper. J.N. performed the bioinformatic analyses, visualized and interpreted results, wrote and revised the paper. Sujeong K. conducted experiments, performed analyses, and interpreted experimental results related to construction of human antibody libraries, ELISA, flow cytometry, gene cloning and expression of recombinant proteins. Y.C. conducted experiments related to gene cloning of RBD mutants and expression of recombinant RBD mutant proteins. D.Y. conducted experiment related to PBMC isolation from human blood sample. M.S. conducted the experiment related to in vitro viral neutralization assay. Y.L. and H.L. performed the bioinformatic analysis. J.J., C.K., K.S., P.C., H.K., E.K., and N.K. contributed to patient recruitment. W.P. conceived the study, designed and conducted experiment related to in vitro viral neutralization assay, and interpreted experimental results. M.O. conceived the study. S.K. conceived the study and designed and supervised the bioinformatics analysis. J.C. conceived the study, designed and supervised all experiments, interpreted all results, and wrote the paper. **Competing interests:** Seoul National University R&DB Foundation is pursuing intellectual property (IP) protection for antibodies reactive to RBD of SARS-CoV-2 and their sequences, of which inventors are J.C., S.K., M.O., W.P., Sang Il K., J.N., Sujeong K., Y.C., D.Y., Y.L., and H.L. All other authors declare no competing interest. **Data and materials availability:** All sequence data were uploaded to the National Center for Biotechnology Information (https://www.ncbi.nlm.nih.gov/) under accession number PRJNA648677. Processed IGH sequence data for the chronological blood samples were uploaded to the iReceptor gateway (https://gateway.ireceptor.org). All other data are included in the manuscript or supplementary materials.

Submitted 7 July 2020
Resubmitted 7 September 2020
Accepted 28 December 2020
Published First Release 4 January 2021
10.1126/scitranslmed.abd6990

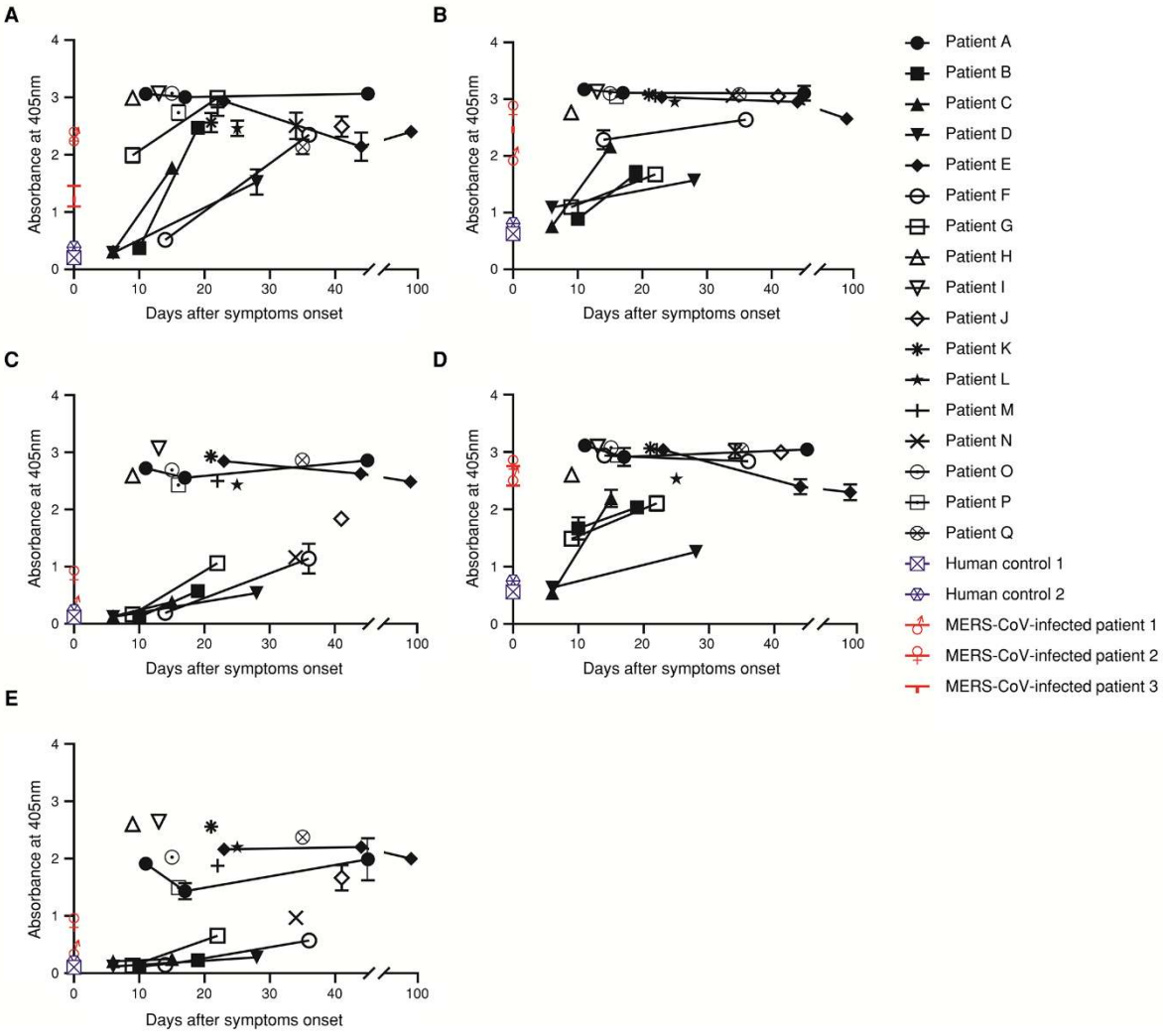

Fig. 1. Titrations of serum IgG by ELISAs specific to SARS-CoV-2. Plasma samples from 17 SARS-CoV-2 patients were diluted (1:100) and added to plates coated with recombinant SARS-CoV-2 **(A)** N, **(B)** S, **(C)** S1, **(D)** S2, which was fused to a polyhistidine (HIS) tag, or **(E)** RBD protein, which was fused to a human C_K domain. The amount of bound IgG was determined using anti-human IgG (Fc-specific) antibody, ABTS was used as the substrate. All experiments were performed in duplicate, and the data are presented as the mean ± SD.

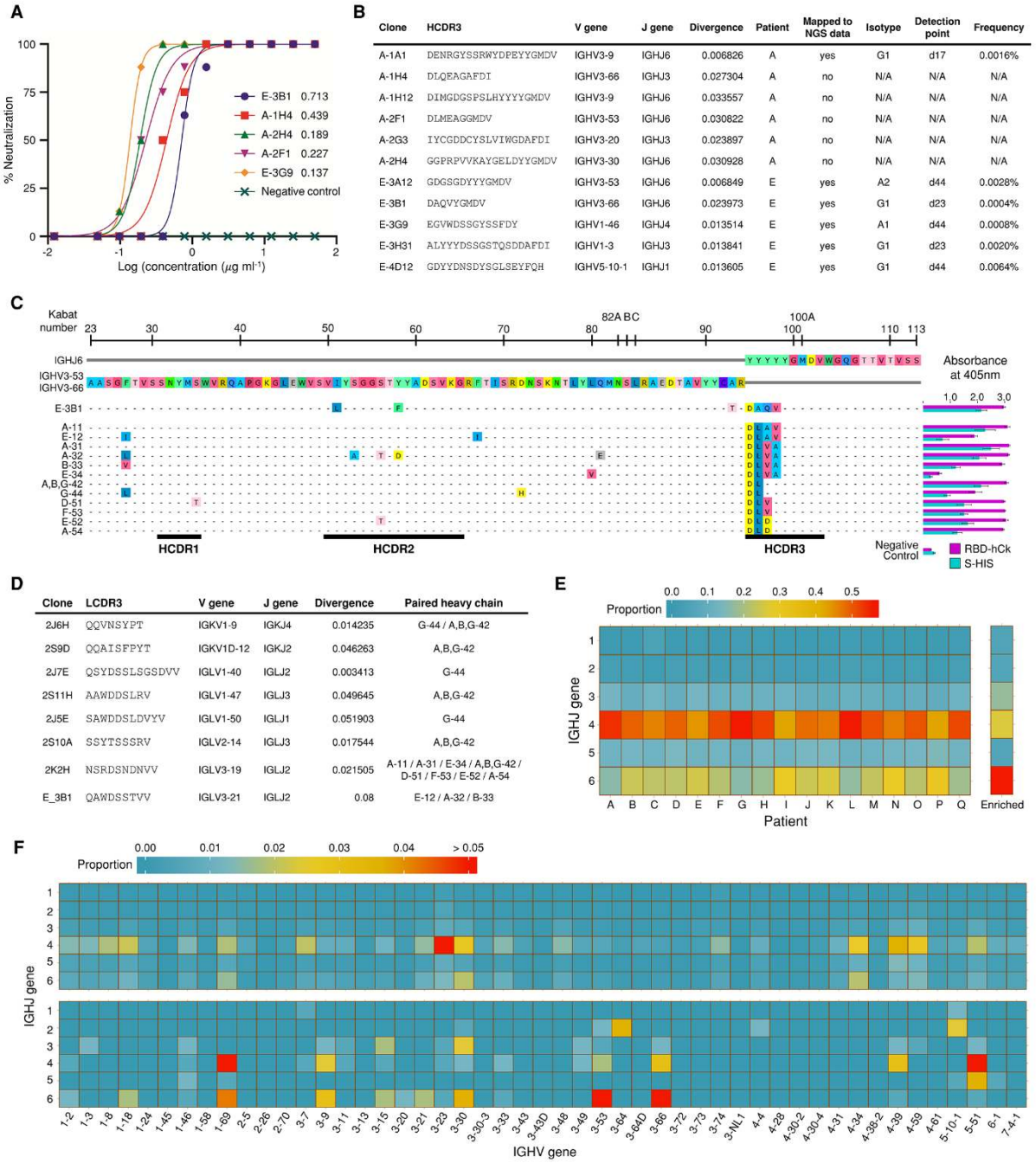

Clone	HCDR3	V gene	J gene	Divergence	Patient	Mapped to NGS data	Isotype	Detection point	Frequency
A-1A1	DENRGYSSRWYDPEYYGMDV	IGHV3-9	IGHJ6	0.006826	A	yes	G1	d17	0.0016%
A-1H4	DLQEAGAFDI	IGHV3-66	IGHJ3	0.027304	A	no	N/A	N/A	N/A
A-1H12	DIMGDGSPSLHYYYYGMDV	IGHV3-9	IGHJ6	0.033557	A	no	N/A	N/A	N/A
A-2F1	DLMEAGGMDV	IGHV3-53	IGHJ6	0.030822	A	no	N/A	N/A	N/A
A-2G3	IYCGDDCYSLVIWGDAFDI	IGHV3-20	IGHJ3	0.023897	A	no	N/A	N/A	N/A
A-2H4	GGPRPVVKAYGELDYYGMDV	IGHV3-30	IGHJ6	0.030928	A	no	N/A	N/A	N/A
E-3A12	GDGSGDYYYGMDV	IGHV3-53	IGHJ6	0.006849	E	yes	A2	d44	0.0028%
E-3B1	DAQVYGMDV	IGHV3-66	IGHJ6	0.023973	E	yes	G1	d23	0.0004%
E-3G9	EGVWDSSGYSSFDY	IGHV1-46	IGHJ4	0.013514	E	yes	A1	d44	0.0008%
E-3H31	ALYYYDSSGSTQSDDAFDI	IGHV1-3	IGHJ3	0.013841	E	yes	G1	d23	0.0020%
E-4D12	GDYYDNSDYSGLSEYFQH	IGHV5-10-1	IGHJ1	0.013605	E	yes	G1	d44	0.0064%

Clone	LCDR3	V gene	J gene	Divergence	Paired heavy chain
2J6H	QQVNSYPT	IGKV1-9	IGKJ4	0.014235	G-44 / A,B,G-42
2S9D	QQAISFPYT	IGKV1D-12	IGKJ2	0.046263	A,B,G-42
2J7E	QSYDSSLSGSDVV	IGLV1-40	IGLJ2	0.003413	G-44
2S11H	AAWDDSLRV	IGLV1-47	IGLJ3	0.049645	A,B,G-42
2J5E	SAWDDSLDVYV	IGLV1-50	IGLJ1	0.051903	G-44
2S10A	SSYTSSSRV	IGLV2-14	IGLJ3	0.017544	A,B,G-42
2K2H	NSRDSNDNVV	IGLV3-19	IGLJ2	0.021505	A-11 / A-31 / E-34 / A,B,G-42 / D-51 / F-53 / E-52 / A-54
E_3B1	QAWDSSTVV	IGLV3-21	IGLJ2	0.08	E-12 / A-32 / B-33

Fig. 2. Characteristics of the isolated nAbs, stereotypic IGH clonotypes, and RBD binding-predicted clones. (A) Serially diluted IgG2/4 was mixed with an equal volume of SARS-CoV-2 containing 100 $TCID_{50}$ and the IgG2/4-virus mixture was added to Vero cells with 8 repeats and incubated for 5 days. Cells infected with 100 $TCID_{50}$ of SARS-CoV-2, isotype IgG2/4 control, or without the virus, were applied as positive, negative, and uninfected controls, respectively. CPE in each well was observed 5 days post-infection. **(B)** Characteristics of nAbs discovered in Patients A and E. **(C)** IGH clonotypes that are highly homologous to E-3B1 and reactive against recombinant SARS-CoV-2 S and RBD proteins. The right column shows the results of the phage ELISA. All experiments were performed in quadruplicate, and the data are presented as the mean ± SD. **(D)** List of diverse IGL clonotypes that can be paired with the IGH clonotypes from (B) to achieve reactivity. **(E)** J and **(F)** VJ gene usage in the IGH repertoire of patients (upper) and the binding-predicted IGH clones (bottom). For the VJ gene usage heatmap, the frequency values for the IGH repertoire of all 17 patients were averaged and are displayed (upper) along with those of the predicted RBD-binding IGH clones (bottom). N/A: not applicable

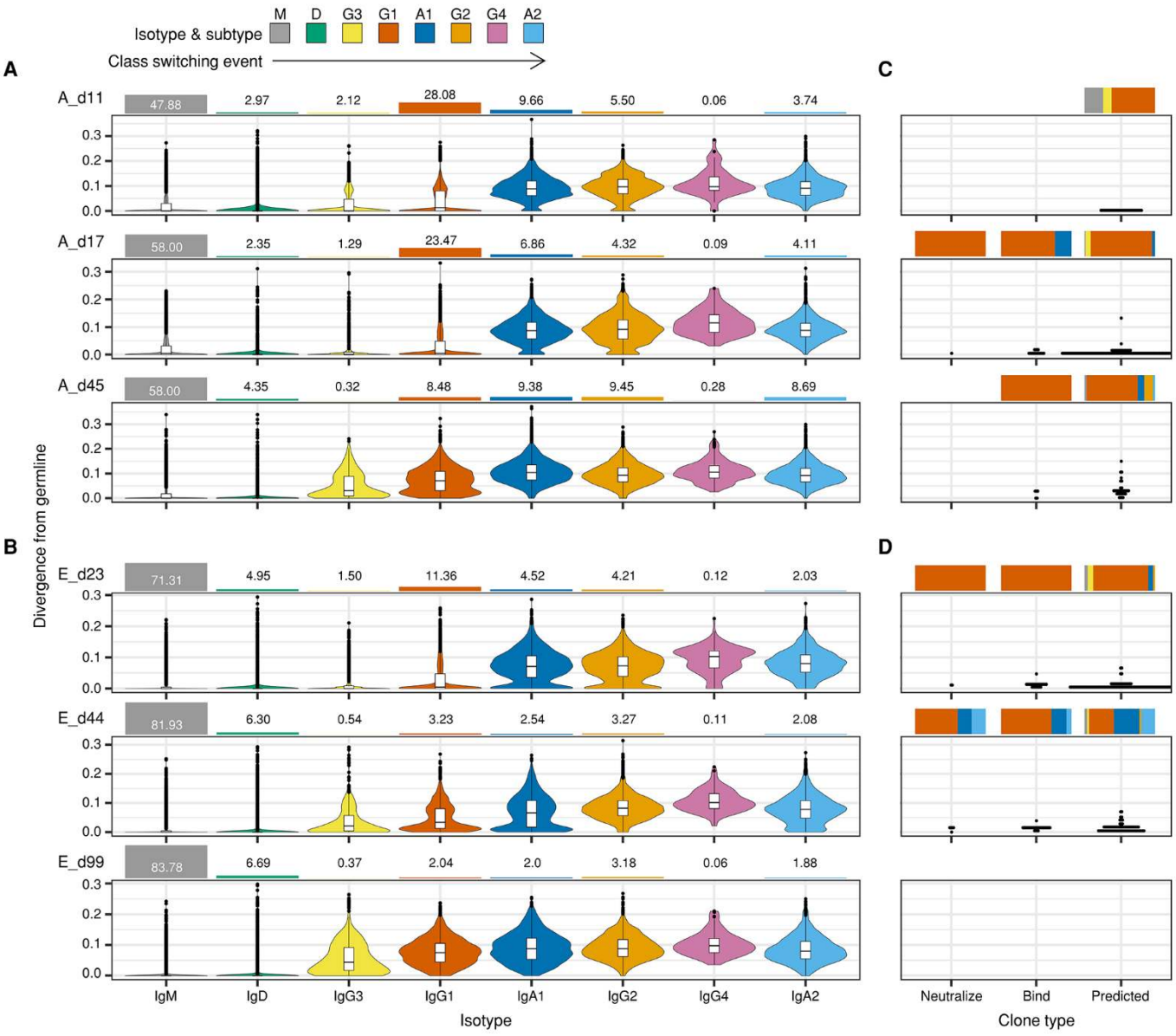

Fig. 3. Deep profiling of the IGH repertoires of Patients A and E. (A and **B)** IGH repertoires of **(A)** Patient A and **(B)** Patient E were analyzed 11, 17, and 45 (A_d11, A_d17, A_d45) days and 23, 44, and 99 (E_d23, E_d44, E_d99) days after symptom onset, respectively. IGH repertoires were examined according to divergence from the germline and the isotype composition of the sequences. Values for divergence from the germline were calculated separately for each isotype and are presented as violin plots, ordered by the class-switch event. The bar graphs on the top of the violin plots represent the proportion of each isotype in the repertoire. **(C** and **D)** Mapping of three types of RBD-binding IGH sequences (neutralize, bind, and predicted), derived from either **(C)** Patient A or **(D)** Patient E, against the corresponding IGH repertoire. The positions of the RBD-binding IGH sequences in the divergence value were annotated as dot plots on the same scale used for (A) and (B). Bar graphs on the top of the dot plots indicate the isotype compositions of the sequences in the repertoire.

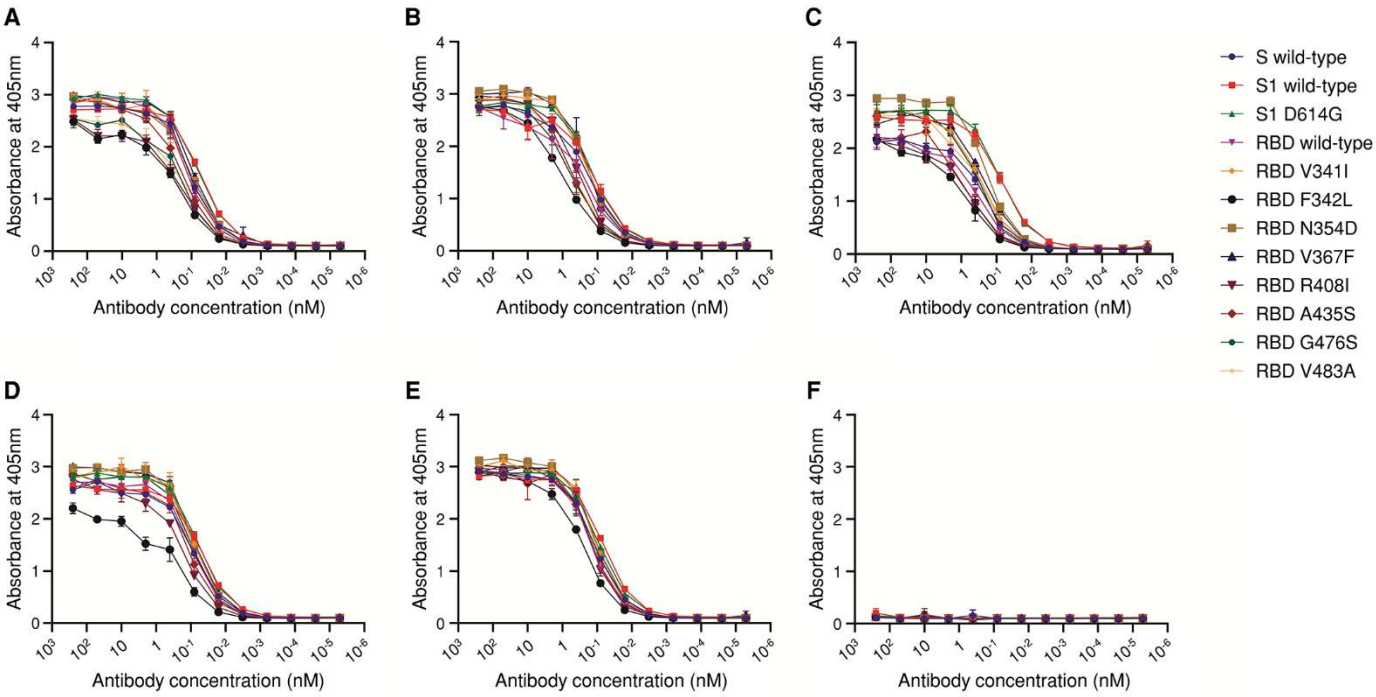

Fig. 4. Reactivity of nAbs against recombinant SARS-CoV-2 spike mutants. Recombinant wild-type or mutant (V341I, F342L, N354D, V367F, R408I, A435S, G476S, V483A, and D614G) SARS-CoV-2 S, S1, or RBD protein-coated microtiter plates were incubated with varying concentrations of **(A)** E-3B1-hFc, **(B)** A-1H4-hFc, **(C)** A-2F1-hFc, **(D)** A-2H4-hFc, **(E)** E-3G9-hFc, and **(F)** irrelevant scFv-hFc. HRP-conjugated anti-human IgG antibody was used as the probe, and ABTS was used as the substrate. All experiments were performed in triplicate, and data are presented as the mean ± SD.

Table 1. The stereotypic V_H clonotypes against SARS-CoV-2 RBD in the healthy population and in SARS-CoV-2-infected patients.

Healthy population						
sample	**V gene**	**J gene**	**CDR3 AA**	**Divergence**	**Isotype**	**Occurrence**
326650	IGHV3-53 / 3-66	IGHJ6	DLYYYGMDV	0.007 ± 0.003	M (100%)	12
326713	IGHV3-53 / 3-66	IGHJ6	DLYYYGMDV	0.005 ± 0.010	M (92.3%), G (7.7%)	13
326780	IGHV3-53 / 3-66	IGHJ6	DLYYYGMDV	0.014 ± 0.010	M (97.4%), G (2.6%)	38
326797	IGHV3-53	IGHJ6	DLYYYGMDV	0.004	M (100%)	1
327059	IGHV3-53 / 3-66	IGHJ6	DLYYYGMDV	0.003 ± 0.005	M (100%)	8
D103	IGHV3-53	IGHJ6	DLYYYGMDV	0.008 ± 0.020	M (100%)	9
326650	IGHV3-53 / 3-66	IGHJ6	DLDYYGMDV	0.006 ± 0.002	M (75%), G (25%)	4
326713	IGHV3-53 / 3-66	IGHJ6	DLDYYGMDV	0.012 ± 0.018	M (100%)	4
326797	IGHV3-66	IGHJ6	DLDYYGMDV	0.055	M (100%)	1
327059	IGHV3-53 / 3-66	IGHJ6	DLDYYGMDV	0.001 ± 0.002	M (100%)	4
D103	IGHV3-53	IGHJ6	DLDYYGMDV	0.053	M (100%)	1
326713	IGHV3-53 / 3-66	IGHJ6	DLVAYGMDV	0.008 ± 0.011	M (100%)	2
326713	IGHV3-53	IGHJ6	DLVYYGDMV	0.001 ± 0.002	M (100%)	3
326797	IGHV3-53	IGHJ6	DLVYYGMDV	0.089 ± 0.008	M (100%)	2
326713	IGHV3-53	IGHJ6	DLVVYGMDV	0.024 ± 0.052	M (100%)	5
326780	IGHV3-53 / 3-66	IGHJ6	DLSYYGMDV	0.024 ± 0.024	M (98.44%), D (0.78%), G (0.78%)	128
D103	IGHV3-53	IGHJ6	DLSYYGMDV	0.022 ± 0.003	M (100%)	2
327059	IGHV3-53	IGHJ6	DLGDYGMDV	0.000	M (100%)	1
326713	IGHV3-66	IGHJ6	DAVSYGMDV	0.000 ± 0.000	M (100%)	2
SARS-CoV-2-infected patients						
sample	**V gene**	**J gene**	**CDR3 AA**	**Divergence**	**Isotype**	**Occurrence**
A	IGHV3-53	IGHJ6	DLYYYGMDV	0.002 ± 0.004	M (5.1%), G1 (94.9%)	59
B	IGHV3-53	IGHJ6	DLYYYGMDV	0.000 ± 0.000	M (33.3%), G1 (66.7%)	3
G	IGHV3-53 / 3-66	IGHJ6	DLYYYGMDV	0.005 ± 0.003	G1 (84.6%), A1 (15.4%)	14
I	IGHV3-53	IGHJ6	DLYYYGMDV	0.000 ± 0.000	M (100%)	4
K	IGHV3-53	IGHJ6	DLYYYGMDV	0.009 ± 0.000	G1 (100%)	2
A	IGHV3-53	IGHJ6	DLAVYGMDV	0.004 ± 0.000	G1 (100%)	2
E	IGHV3-66	IGHJ6	DLAVYGMDV	0.018 ± 0.000	G1 (100%)	6
A	IGHV3-53	IGHJ6	DLDYYGMDV	0.000 ± 0.000	G1 (100%)	3
E	IGHV3-53	IGHJ6	DLDYYGMDV	0.004 ± 0.000	A1 (100%)	4
I	IGHV3-66	IGHJ6	DLDYYGMDV	0.002 ± 0.003	G1 (100%)	5
K	IGHV3-53	IGHJ6	DLDYYGMDV	0.007 ± 0.005	G1 (100%)	107
M	IGHV3-53	IGHJ6	DLDYYGMDV	0.018	G1 (100%)	1
A	IGHV3-53	IGHJ6	DLVAYGMDV	0.008 ± 0.017	G1 (100%)	14
B	IGHV3-53	IGHJ6	DLVAYGMDV	0.009	G1 (100%)	1
E	IGHV3-53	IGHJ6	DLVAYGMDV	0.005 ± 0.002	G1 (100%)	6
D	IGHV3-53	IGHJ6	DLVYYGMDV	0.004	G1 (100%)	1
E	IGHV3-53	IGHJ6	DLVYYGMDV	0.013	A1 (100%)	1
F	IGHV3-53	IGHJ6	DLVYYGDMV	0.001 ± 0.003	M (75%), G1 (25%)	16
B	IGHV3-53	IGHJ6	DLVVYGMDV	0.002 ± 0.002	M (27.3%), G1 (72.7%)	11
E	IGHV3-53	IGHJ6	DLVVYGMDV	0.013 ± 0.000	A2 (100%)	4
H	IGHV3-53	IGHJ6	DLVVYGMDV	0.009 ± 0.000	G1 (100%)	7
A	IGHV3-53	IGHJ6	DLSYYGMDV	0.013 ± 0.016	G1 (100%)	5
F	IGHV3-53	IGHJ6	DLSYYGMDV	0.018	G1 (100%)	1
O	IGHV3-53	IGHJ6	DLSYYGMDV	0.000	G1 (100%)	1
A	IGHV3-53	IGHJ6	DLGDYGMDV	0.009 ± 0.000	G1 (100%)	3
E	IGHV3-53	IGHJ6	DLGDYGMDV	0.018 ± 0.019	G1 (85.7%), A1 (14.3%)	7
F	IGHV3-53	IGHJ6	DLGDYGMDV	0.003 ± 0.002	M (92.0%), G1 (8.0%)	163
H	IGHV3-53	IGHJ6	DLGDYGDMV	0.004 ± 0.000	G1 (100%)	8
G	IGHV3-53	IGHJ6	DAVSYGMDV	0.004 ± 0.004	M (7.0%), G1 (93.0%)	57
I	IGHV3-53	IGHJ6	DAVSYGMDV	0.007 ± 0.003	G1 (100%)	9
P	IGHV3-53	IGHJ6	DAVSYGMDV	0.000 ± 0.000	G1 (100%)	3

E	IGHV3-53	IGHJ6	DLGPYGMDV	0.009	G1 (100%)	1
I	IGHV3-53 / 3-66	IGHJ6	DLGPYGMDV	0.010 ± 0.003	G3 (40%), G1 (40%), A1 (20%)	4
A	IGHV3-53	IGHJ6	DLVIYGMDV	0.003 ± 0.004	M (5.9%), G1 (94.1%)	17
I	IGHV3-66	IGHJ6	DLVIYGMDV	0.007 ± 0.004	G1 (100%)	8
E	IGHV3-53 / 3-66	IGHJ6	DLVVLGMDV	0.009 ± 0.000	A2 (100%)	20
I	IGHV3-53	IGHJ6	DLVVLGMDV	0.000	G1 (100%)	1

The healthy population samples based on publicly available IGH repertoires or patient identification can be found in the sample column. Clonotypes were mapped according to identical VJ gene usage of IGHV3-53/IGHV3-66 and IGHJ6 and perfectly matched HCDR3 amino acid sequences. Read counts of the mapped sequences in the repertoires of each sample were annotated in the occurrence column. For clonotypes with multiple occurrences, the mean and standard deviation of divergence were represented. The proportion of each isotype is indicated for each sample as a percentage.